Artificial Interphase Design Employing Inorganic–Organic Components for High-Energy Lithium-Metal Batteries

Yongil Kim, Dominik Stepien, Hyein Moon, Kay Schönherr, Benjamin Schumm, Matthias Kuenzel, Holger Althues, Dominic Bresser,* and Stefano Passerini*

ABSTRACT: To increase the energy density of today's lithium batteries, it is necessary to develop an anode with higher energy density than graphite or carbon/silicon composites. Hence, research on metallic lithium has gained a steadily increasing momentum. However, the severe safety issues and poor Coulombic efficiency of this highly reactive metal hinder its practical application in lithium-metal batteries (LMBs). Herein, the development of an artificial interphase is reported to enhance the reversibility of the lithium stripping/plating process and suppress the parasitic reactions with the liquid organic carbonate-based electrolyte. This artificial interphase is spontaneously formed by an alloying reaction-based coating, forming a stable inorganic/organic hybrid interphase. The accordingly modified lithium-metal electrodes provide substantially improved cycle life to symmetric Li||Li cells and high-energy Li||$LiNi_{0.8}Co_{0.1}Mn_{0.1}O_2$ cells. For these LMBs, 7 μm thick lithium-metal electrodes have been employed while applying a current density of 1.0 mA cm^{-2}, thus highlighting the great potential of this tailored interphase.

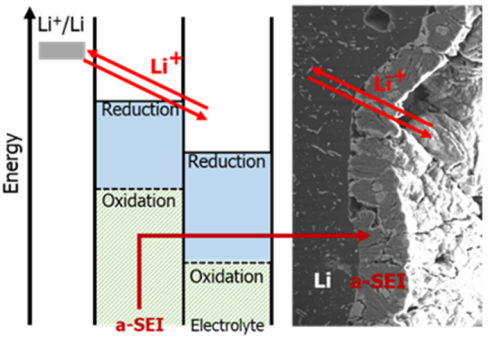

KEYWORDS: *artif icialinterphase, lithium metal, tin chloride, lithium nitrate, battery*

INTRODUCTION

The market for lithium-ion batteries (LIBs) continues to grow, driven by the increasing demand for electric vehicles and energy storage devices.[1−4] However, LIBs are about to reach their performance limits, and although the demand for high-performance and low-cost energy storage devices is increasing, the improvements in energy and power density are rather incremental frequently.[5−7] Substantial progress requires either strikingly new design concepts or the introduction of new electrode materials. Concerning the latter, one of the most promising options is the use of metallic lithium at the negative electrode, owing to its high theoretical specific capacity of 3860 mAh g^{-1} and low redox potential of −3.04 V vs the standard hydrogen electrode (SHE).[8−13] In fact, rechargeable lithium-metal batteries (LMBs) had been commercialized already in the 1980s,[14,15] but the severe safety issues related to the formation of lithium dendrites and the continuous decomposition of the electrolyte at the interface with the lithium metal electrode resulted in a rather poor cycle life preventing the widespread commercial use, eventually.[16−18] The continuous electrolyte decomposition originates from the electrochemical potential of metallic lithium being well beyond the electrochemical stability window of common organic solvent-based liquid electrolytes. While a stable passivation layer—also known as solid electrolyte interphase (SEI)—forms on graphite, i.e., the state-of-the-art active material for the negative electrode in LIBs, the same does not occur in LMBs, where the metal anode undergoes essentially unlimited volume changes upon dis-/charge rendering this challenge dramatically more difficult.[9,19,20] In fact, an ideal passivation layer with the function of an SEI allows Li^+ cations to permeate while preventing any electron transport.[9,21] In addition, it needs to remain unaffected by the continuous volume changes of the lithium-metal anode and provide a mechanically, chemically, and electrochemically stable interface with the electrolyte. Moreover, it must suppress the dendritic lithium deposition and enable homogeneous lithium plating and stripping.

In the past years, several approaches have been proposed to address these issues and challenges, including the introduction of functional electrolyte additives,[22] the application of advanced current collector architectures,[23−25] and the design of (in situ formed) artificial interphases.[9,26−31] Among the various strategies to yield the in situ formation of a suitable artificial interphase, intermetallic compounds, involving metals that can form an alloy with lithium, e.g., In, Bi, Sn, Sb, or Ag (and the corresponding metal halides as precursors), have attracted particular interest.[32−43] An advantage of such lithium-

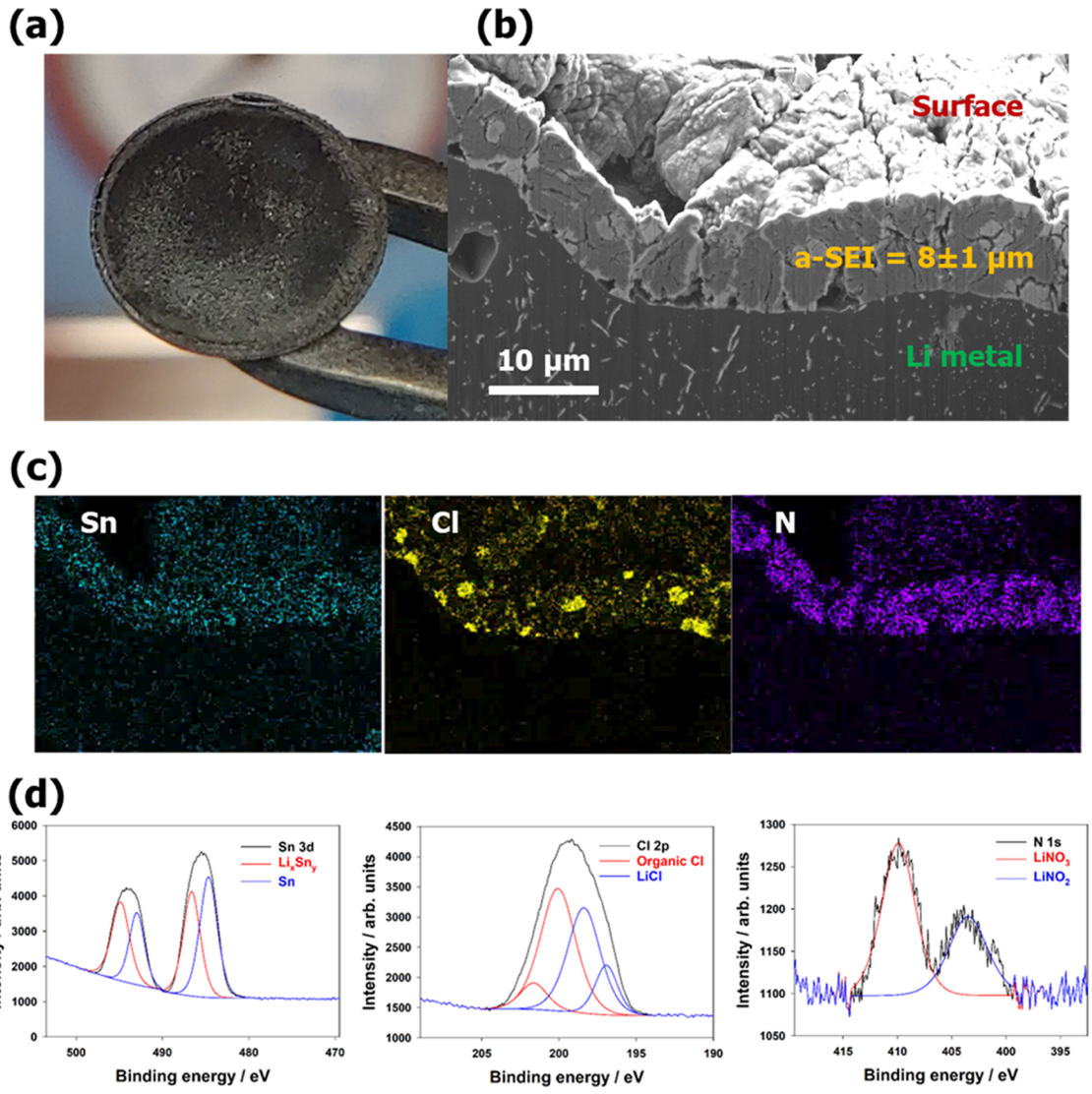

Figure 1. (a) Photograph of the lithium foil after coating with the $SnCl_2$ and $LiNO_3$ in DME solution and removal of the solvent by evaporation. (b) SEM micrograph of the cross section of a-SEI-Li (original thickness of the lithium foil: 300 μm). (c) Corresponding EDX mapping for Sn, Cl, and N (from left to the right). (d) Detailed XPS spectra region (from left to right: Sn 3d, Cl 2p, and N 1s) of a-SEI-Li.

comprising intermetallic compounds is the commonly facile lithium transport within and across such interphases. Besides, the introduction of functional additives to form a stable interphase has attracted even greater attention. One of the most common additives is lithium nitrate ($LiNO_3$).[44−47] When $LiNO_3$ gets in contact with the lithium metal surface, it is reduced to lithium nitride (Li_3N) and lithium oxynitrides (LiN_xO_y).[48,49] The resulting passivation layer significantly reduces dendritic lithium deposition and enables highly effective lithium stripping and plating.[49] It appears noteworthy, though, that, owing to its very limited solubility in, e.g., organic carbonates,[50] the use of $LiNO_3$ is limited to ether-based electrolytes, which are incompatible with 4 V cathodes due to the rather poor oxidation stability of ether-type solvents.[51]

Herein, we report a facile approach for a novel artificial interphase on the surface of lithium-metal anodes in LMBs that combines these two approaches. Tin chloride ($SnCl_2$) and $LiNO_3$ were used as precursors for the artificial interphase, which comprises lithium−tin intermetallic compound (Li_xSn_y), lithium chloride (LiCl), as well as Li_3N and LiN_xO_y. The approach relies on the use of an ether-type solvent for the artificial interphase formation, which provides the additional advantage of a simple removal by evaporation. Such an artificial interphase provides a greatly enhanced cycling stability of symmetric Li||Li cells and high-energy Li||$LiNi_{0.8}Co_{0.1}Mn_{0.1}O_2$ cells, both using organic carbonate-based liquid electrolytes. The LMBs have been tested employing a lithium-metal anode as thin as 7 μm at current densities as high as 1.0 mA cm^{-2}.

EXPERIMENTAL METHODS

Preparation of the Artificial Interphase on Lithium Metal. The preparation of the artificial interphase was carried out in an argon-filled glovebox. Lithium-metal foils with a thickness of 300, 50, and 20 μm (Honjo) as well as 10 and 7 μm (see the next paragraph for a description of the preparation) were coated using a 0.1 M solution of $SnCl_2$ (min. 99%, Alfa Aesar) in dimethoxyethane (DME) with 2 wt % $LiNO_3$ (99.999%, Alfa Aesar). In some specific experiments (see details in the article), $LiNO_3$ was not added to the coating solution. The lithium foil was allowed to react for 30 min prior to the removal of DME by evaporation.

Preparation of the 10 and 7 μm Thin Lithium Foil. The Fraunhofer Institute for Material and Beam Technology (IWS) developed a lithium melt deposition process for preparing very thin

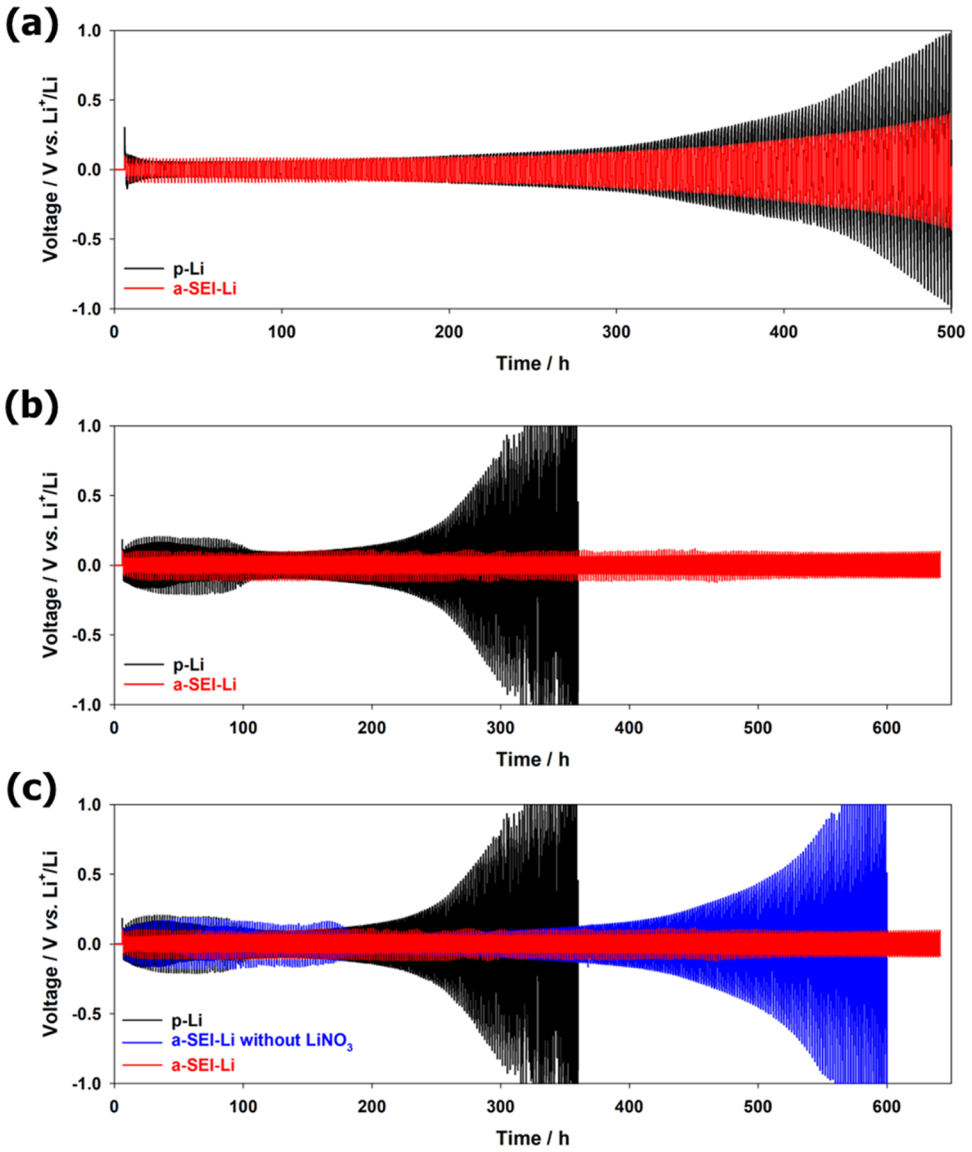

Figure 2. Galvanostatic lithium stripping/plating experiments performed on symmetric Li||Li cells at a current density of 1.0 mA cm^{-2}, comprising a-SEI-Li (in red) and p-Li (in black). Stripping/plating experiments using (a) 1.2 M $LiPF_6$ in EC:EMC (3:7 wt %) and (b) 1.2 M $LiPF_6$ in EC:EMC (3:7 wt %) + 5 wt % VC as the electrolyte. (c) Comparison of the data presented in panel (b) with a symmetric Li||Li cell employing Li electrodes treated with $SnCl_2$ only, i.e., without $LiNO_3$ (in blue). Each stripping/plating step lasted for 1 h, resulting in a total capacity of 1.0 mAh cm^{-2} per step. Initial Li foil thickness: 300 μm; electrolyte: 60 μL; temperature: 20 ± 1 °C.

lithium films on copper foils. This process is based on the realization of a lithiophilic surface on the copper substrate, enhancing the liquid lithium wetting. The two lithium films studied herein were deposited on a 12 μm thick copper foil (SE-Cu58, Cu: ≥99.9%, P: ≤0.006%, Schlenk), which was treated at 300 °C for 60 s in a laboratory air atmosphere using a roll-to-roll (R2R) furnace (HTM Reetz). As a result of this thermal treatment, a ∼200 nm thin Cu_2O layer was formed.[52] The thus treated copper foil substrate (width: 150 mm, length: 2 m) was coated with molten lithium (purity: 99.95%, Cellithium) using a liquid lithium coating setup (described elsewhere[52]) with a vessel temperature of 205 °C under the argon atmosphere inside a glovebox with <0.1 ppm H_2O, <0.1 ppm O_2, and <10 ppm N_2. The substrate velocity was set to 600 mm min^{-1} for 10 μm thick Li films and 400 mm min^{-1} for 7 μm thick Li films by a R2R winding.

Physicochemical Characterization. Scanning electron microscopy (SEM) was conducted using a ZEISS Crossbeam XB340 equipped with an EDX detector. For the investigation of the cross section, a Capella-focused ion beam (FIB) with a gallium ion source was used. X-ray photoelectron spectroscopy (XPS) was carried out utilizing a SPECS UHV system (FOCUS 500 equipped with a monochromatic X-ray source, PHOIBOS 150 hemispherical energy analyzer with 2D DLD detector) using the Al Kα ($h\nu$ = 1486.6 eV) radiation. Deconvolution of the XPS peaks was performed using the software CasaXPS. A standard Shirley-type background was used, and a mixed Gaussian−Lorentzian type fitting was applied to the peaks.

Electrochemical Characterization. Unless otherwise stated, the 1.2 M solution of $LiPF_6$ in EC/EMC (3:7 wt %) + 5 wt % VC was used as the electrolyte. The positive electrodes based on $LiNi_{0.8}Co_{0.1}Mn_{0.1}O_2$ (NCM_{811}) as the active material were prepared by blending NCM811 (92 wt %; POSCO CHEMICAL CO., LTD), C-NERGY carbon black (4 wt %; Imerys), and poly(vinylidene difluoride) (PVdF 6020, 4 wt %; Solvay) in *N*-methyl-2-pyrrolidone (NMP, Aldrich). The resulting slurry was coated on a Al foil (battery grade) and pre-dried at 60 °C. Subsequently, disk-shaped electrodes were punched with a diameter of 12 mm. The electrode disks were dried at 110 °C under the vacuum overnight. The average active material (NCM_{811}) mass loading was around 15.7 ± 0.3 mg cm^{-2}.

Electrochemical measurements were conducted using CR2032-type coin cells employing (bare/coated) lithium disks with a diameter of 12 mm as the negative electrode, NCM_{811}-based positive electrodes with a diameter of 12 mm, trilayer PE/PP separators (Asahi Kasei) with a diameter of 19 mm, and 60 μL of the liquid electrolyte in each cell. For the Li||Cu cells, Cu foils (Schlenk) with a diameter of 12 mm were used as the working electrodes. For the determination of the limiting current density, the BioLogic VMP potentiostat and three-electrode Swagelok-type T-cells were used, employing lithium metal foil as the reference electrode. Galvanostatic measurements were conducted with a Maccor 4000 battery tester. Electrochemical impedance spectroscopy (EIS) was performed using a BioLogic VMP potentiostat equipped with an impedance module while varying the frequency from 1 MHz to 100 mHz with a voltage amplitude of 10 mV.

RESULTS AND DISCUSSION

Application and Composition of the Artificial Interphase. The artificial solid electrolyte interphase (a-SEI) was applied by a facile coating process employing $SnCl_2$ and $LiNO_3$ precursors dissolved in dimethoxyethane (DME). After removing the DME via evaporation, the surface of the lithium metal turned black (Figure 1a). The analysis of the cross section by scanning electron microscopy (SEM) reveals the formation of a surface layer on top of the lithium metal with a thickness of about 8 ± 1 μm (Figure 1b). This surface layer, herein referred to as a-SEI, provides a homogeneous coverage of the lithium metal foil although showing a few cracks presumably related to the solvent evaporation. Energy dispersive X-ray (EDX) mapping shows a rather uniform distribution of Sn, Cl, and N in a-SEI (Figures 1c and S1). Only the Cl mapping indicates some larger agglomerates. Further analysis of the composition of a-SEI was conducted by X-ray photoelectron spectroscopy (XPS, Figure 1d). The peaks observed in the Sn 3d spectrum are assigned to Li_xSn_y and Sn, the peaks observed in the Cl 2p spectrum are assigned to organic chloride compounds and LiCl,[34,39,53−56] and the peaks found in the N 1s spectrum are attributed to the presence of $LiNO_3$ and $LiNO_2$.[57] Accordingly, a-SEI is composed of Li_xSn_y, Sn, organic chloride compounds, LiCl, $LiNO_3$, and $LiNO_2$ as a result of the spontaneous reaction of $SnCl_2$, $LiNO_3$, and DME with lithium metal. Such composition enables the stabilization of the electrodelelectrolyte interface by lowering the energy of the components that are in direct contact with the electrolyte, as schematically illustrated in Figure S2. However, this spontaneously formed a-SEI provides high lithium-ion conductivity owing to the presence of $LiNO_x$ and LiCl and good stability toward metallic lithium.[58,59]

Characterization in Symmetric Li||Li Cells. To investigate the effect of a-SEI on the electrochemical behavior of the lithium-metal electrodes, symmetric Li||Li cells employing pristine Li electrodes (p-Li) or a-SEI-coated Li electrodes (a-SEI-Li) were assembled and compared via a series of electrochemical tests. In the first step, lithium stripping/plating tests at a current density of 1.0 mA cm^{-2} were performed using 1.2 M $LiPF_6$ in a 3:7 (wt) mixture of ethylene carbonate (EC) and ethyl methyl carbonate (EMC) as the electrolyte (Figure 2a). The comparison of the two symmetric cells reveals a substantially reduced increase of the overpotential during stripping/plating for a-SEI-Li. The p-Li cell shows a rapidly rising overpotential after 400 h (200 cycles), indicating the formation of a highly resistive surface layer and/or electrolyte depletion owing to the continuous exposure of fresh lithium metal surface.[60] Such rapid increase, however, did not occur when a-SEI-Li was employed, but only a gradual increase of overpotential upon cycling. Additionally, the application of a-SEI to Li electrodes led to a much lower overpotential for the initial stripping/plating cycles, indicating its beneficial impact on the charge transfer at the electrode/electrolyte interface. The difference is even greater when introducing vinylene carbonate (VC) as an electrolyte additive (Figure 2b). The Li||Li cell comprising p-Li shows a dramatic increase in overpotential after only 250 h (125 cycles), while the symmetric cell containing a-SEI-Li does not show any significant increase in overpotential for more than 600 h. These results suggest a beneficial interaction of a-SEI and the VC additive, which is known to form a polymeric surface layer when reductively decomposed.[61−63]

Figure 2c depicts the deconvolution of the impact of the two a-SEI precursors by comparing the results presented in Figure 2b with those of a symmetric Li||Li cell that was treated with a solution of $SnCl_2$ only, i.e., in the absence of $LiNO_3$. While the cycling stability of the $SnCl_2$-treated Li electrodes is superior to that of p-Li, it is clearly inferior to the a-SEI-Li, as the rapid increase in overpotential is only delayed but not avoided. Thus, the simultaneous presence of $SnCl_2$ and $LiNO_3$ is essential for the formation of a highly stable interface and interphase and suppressed electrolyte decomposition, resulting in stable overpotentials upon long-term cycling. Advantageous in this regard is the insolubility of $LiNO_x$ species in organic carbonate-based electrolytes, ensuring the stability of a-SEI.

The beneficial impact of a-SEI becomes even more obvious when increasing the duration of each stripping/plating step from 1 to 3 h, i.e., the total capacity per step from 1 to 3 mAh cm^{-2} (Figure S3a). In fact, a dramatic increase in overpotential occurs for the symmetric cell with p-Li after only 41 cycles (250 h), while a very stable overpotential is observed for a-SEI-Li upon 133 cycles (800 h). Similarly, the symmetric cell comprising a-SEI-Li shows a substantially improved performance and much lower overpotential when stepwise increasing the current density applied from 1.0 to 3.0 mA cm^{-2} (Figure S3b). The cell comprising p-Li faded rather rapidly when applying a current density of 3.0 mA cm^{-2}, while the cell employing a-SEI-Li showed a rather stable overpotential throughout the whole experiment. This superior behavior originates from a better charge transfer at the interface/across the interphase, as also reflected by the determination of the current density when sweeping the voltage of the symmetric cells (Figure S3c). While the current density at 0.2 V, for instance, amounts to 1.96 mA cm^{-2} for p-Li, it was substantially higher with 3.32 mA cm^{-2} in the case of a-SEI-Li. In other words, the application of a certain current density to the cell results in a much lower overpotential in the presence of a-SEI.

In the next step, the symmetric cells were subjected to galvanostatic stripping/plating experiments combined with electrochemical impedance spectroscopy (EIS) to better understand the impact of a-SEI on the charge transfer and transport across the interface and interphase, respectively. The stripping/plating experiment results are presented in Figure S4a together with the points at which EIS measurements were performed (i.e., before stripping/plating as well as after the 1st, 10th, and 30th cycle). The corresponding EIS results are depicted in Figure S5a−d. It is immediately apparent that the impedance is generally much lower for the a-SEI-Li, especially before plating/stripping (Figure S5a). Upon cycling, the difference decreases since the impedance gets lower for the

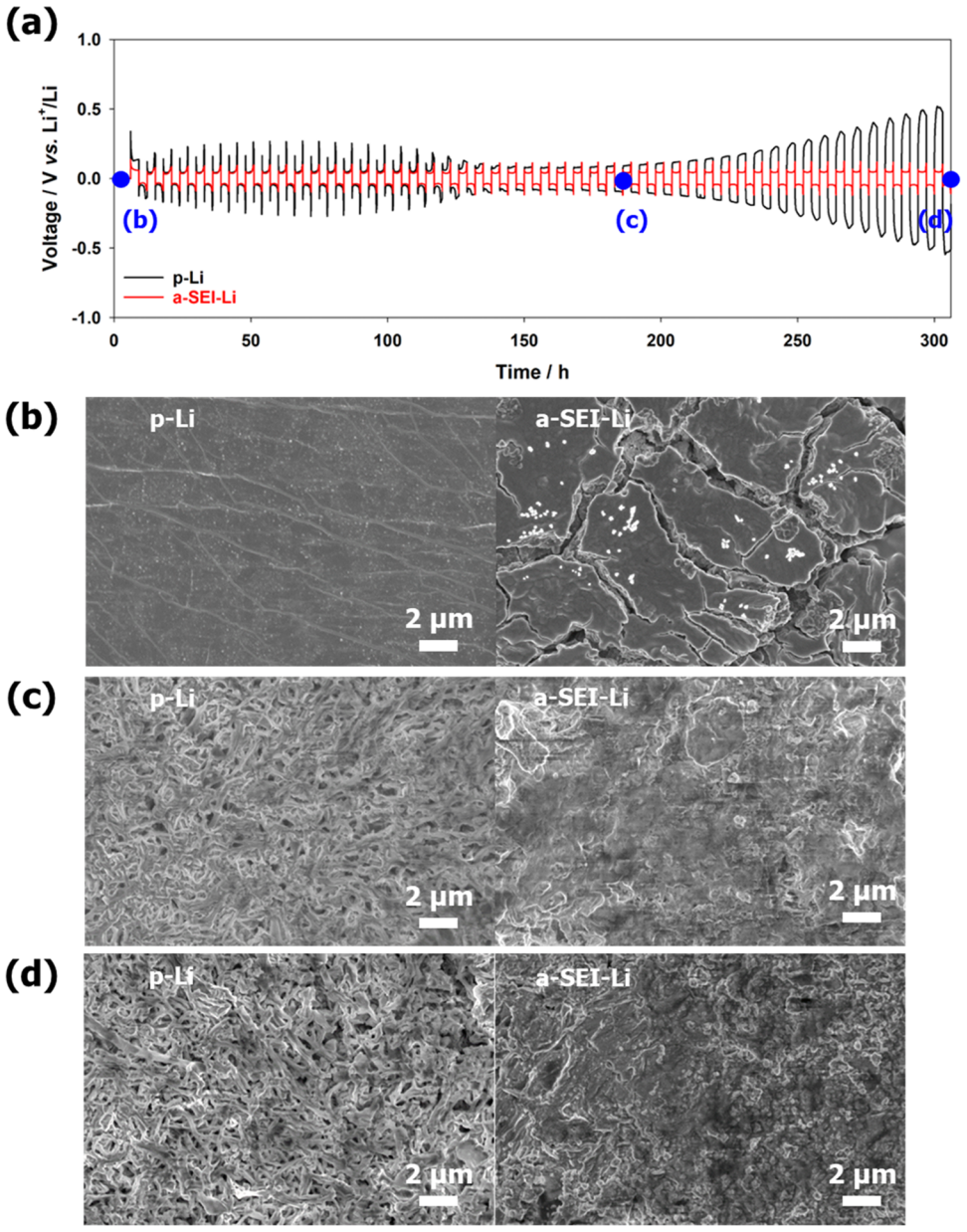

Figure 3. (a) Galvanostatic lithium stripping/plating experiments performed for symmetric Li||Li cells at a current density of 1.0 mA cm^{-2} (each stripping/plating step lasting for 3 h, resulting in a total capacity of 3.0 mAh cm^{-2}), comprising a-SEI-Li (in red) and p-Li (in black), combined with an ex situ SEM analysis of the pristine electrodes as well as after 30 and 50 cycles, as indicated. (b–d) Corresponding SEM micrographs of p-Li (left) and a-SEI-Li (right) in (b) the pristine state, (c) after 30 cycles, and (d) after 50 cycles. Initial Li foil thickness: 300 μm; electrolyte: 60 μL; temperature: 20 ± 1 °C.

p-Li cell and slightly higher for the a-SEI-Li cell (Figure S5b–d). For a more detailed analysis, the impedance spectra were fitted with an equivalent circuit (Figure S4b). The results from the fitting are provided in Table S1 and plotted in Figure S5e. The equivalent circuit components R_b, R_{SEI}, and R_{ct} represent the bulk (electrolyte and electrode), the SEI, and the charge transfer resistances, respectively.[64,65] The total resistance, referred to as R_{total}, is the sum of R_b, R_{SEI}, and R_{ct}. Prior to the stripping/plating test, the cell comprising p-Li had a much higher R_{total} (755.9 Ω·cm^2) than that employing a-SEI- Li (93.8 Ω·cm^2), mostly owing to substantially higher R_{SEI} and R_{ct}. These are related to the resistive native surface layer on p-Li, consisting of Li_2CO_3, Li_2O, and LiOH.[46] After one stripping/plating cycle, R_{total} decreased for both cells, though far more for the p-Li one, which is attributed to the reconstruction of the native surface layer into a more conductive SEI based on the substantial decrease of R_{SEI} and R_{ct} (Figure S5e). In the case of the a-SEI-Li cell, R_{ct} decreased as well, which is attributed to potential Li trapping in a-SEI, thus facilitating charge transport. In both cases, R_b remained essentially constant after the first cycle but increased slightly in the following cycles, especially, for p-Li, indicating an ongoing depletion of the electrolyte. As R_b includes also the resistance within the lithium metal electrode, the greatest increase for p-Li might indicate more pronounced changes—which are suppressed to a certain extent in a-SEI-Li.[60] To investigate this, an ex situ SEM analysis of p-Li and a-SEI-Li was performed. Exemplary stripping/plating experiments are presented in Figure 3a. SEM micrographs were taken on the electrodes prior to the plating/stripping test (Figure 3b), after 30 cycles (Figure 3c), and after 50 cycles

(Figure 3d) (for each experiment, one new cell was assembled). Prior to the plating/stripping test (Figure 3b), p-Li shows a very smooth surface, whereas a-SEI-Li exhibits a rather cracked (crusty) surface in line with the cross-sectional SEM micrograph shown in Figure 1b. Upon cycling, however, the morphology of p-Li becomes increasingly porous, while the surface of a-SEI- Li becomes very dense and rather homogeneous (Figure 3c,d). It appears that the initial cracks are filled with electrochemically derived SEI products—e.g., stemming from the reductive decomposition of VC yielding polymeric SEI components—resulting in the formation of a stable interphase. Differently, the increasing porosity of p-Li indicates the absence of a stable interphase. These changes agree with the increase in R_b. In the case of p-Li, the fluctuating values for R_{SEI} and R_{ct} are presumably resulting from the contrasting impact of the increased surface area and the accumulation of resistive electrolyte decomposition products, leading to a decrease and increase of the two resistance contributions, respectively. Generally, these results highlight the beneficial effect of a-SEI on the stripping/plating behavior of a-SEI-Li, particularly in combination with VC as an electrolyte additive.

Evaluation in Li\|\|NCM_{811} Full-Cells. Taking advantage of the highly beneficial effect of a-SEI observed for symmetric Li\|\|Li cells, the impact on the performance of Li\|\|$LiNi_{0.8}Co_{0.1}Mn_{0.1}O_2$ (Li\|\|NCM_{811}) full-cells was investigated. The active material mass loading of the NCM_{811} positive electrode was set to about 15.7 mg cm^{-2} to obtain meaningful insights for current densities that are of relevance in commercial cells. The comparison of the full-cells comprising p-Li and a-SEI-Li as the negative electrode (Figure 4) shows the dramatic beneficial effect of a-SEI on the electrochemical performance. The cell containing a-SEI-Li exhibits high reversible capacity (around 3.0 mAh cm^{-2}) and substantial cycling stability over 250 cycles at a current density of 1.0 mA cm^{-2} (Figure 4a). Differently, the p-Li-based cell shows rather stable cycling for only 50 cycles. The corresponding dis-/charge profiles for the cell based on p-Li and a-SEI-Li are presented in Figure 4b,c, respectively. It is observed that the rapid fading of the former is related to the great polarization increase (Figure 4b), which does not occur for the a-SEI-Li cell even after 250 cycles (Figure 4c).

Extension to Very Thin Lithium Foils. Following the use of NCM_{811} positive electrodes with commercial-like high mass loading, the study was extended to thinner lithium foils with a thickness of 50, 20, 10, and 7 μm to reduce the lithium excess in the cell.[66−68] While the first two lithium foils are commercial products, the latter two lithium foils were prepared by a newly developed process based on the application of a lithiophilic surface on the copper foil and the subsequent deposition of molten metallic lithium.[52] An SEM micrograph of the cross section of the thinnest lithium foil (7 μm) is presented in Figure S6. For this foil, the formation of a-SEI led to the almost complete consumption of the lithium metal (Figure S7a), i.e., the reaction with $SnCl_2$ and $LiNO_3$ proceeds throughout the whole lithium layer, resulting in a rather grain-like morphology and a relatively rough surface. The almost complete reaction is also evidenced by the homogeneous distribution of Sn, Cl, N, and O in a-SEI, as observed via EDX mapping (Figure S7b).

The a-SEI-Li made from Li foils of different thicknesses were subjected to galvanostatic stripping/plating experiments in symmetric Li\|\|Li cells. The results for the 50, 7, 20, and 10 μm thick lithium foil are presented in Figures 5a,b, and S8a−c,

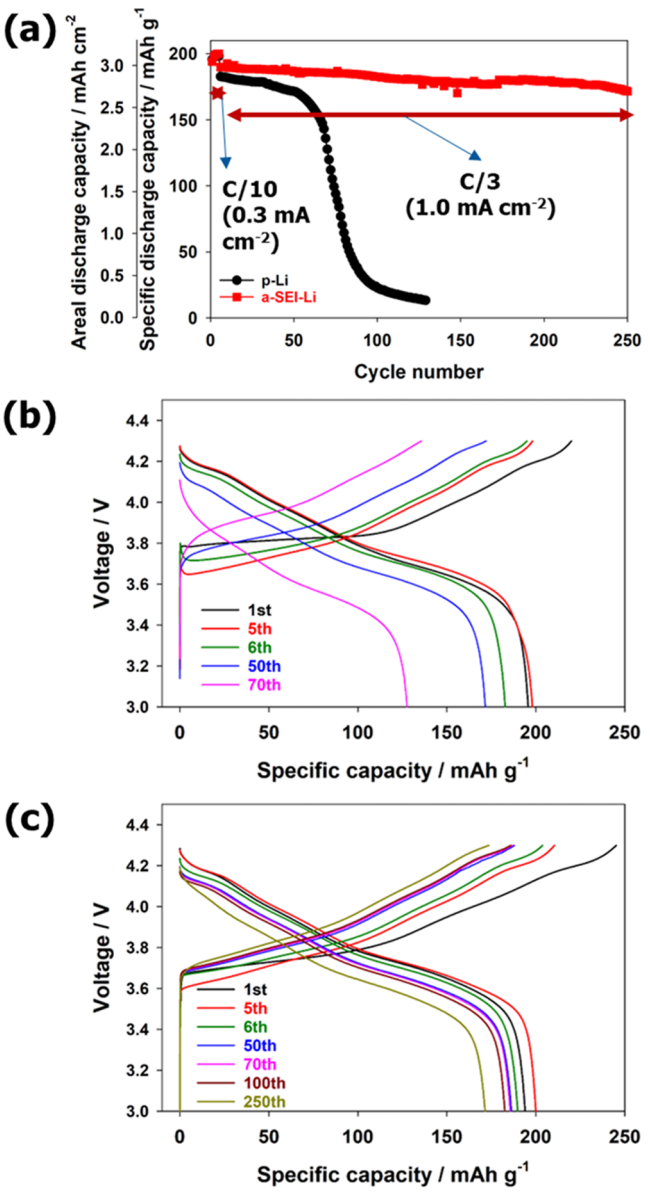

Figure 4. Galvanostatic cycling of (a-SEI-coated) Li\|\|NCM_{811} cells: (a) Plot of the areal and specific discharge capacity as a function of the cycle number for the cell comprising p-Li (in black) and a-SEI-Li (in red). Selected dis-/charge profiles for the p-Li cell (b) and the a-SEI-Li cell (c). For the initial five cycles, the applied current density was 0.3 mA cm^{-2} (C/10), followed by a current density of 1.0 mA cm^{-2} (C/3) for the subsequent cycles. Initial Li foil thickness: 300 μm; NCM_{811} areal loading: 15.7 ± 0.3 mg cm^{-2}; electrolyte: 60 μL; temperature: 20 ± 1 °C.

respectively. Comparing the cells comprising 50 μm thick (areal capacity of ca. 10 mAh cm^{-2}) p-Li and a-SEI-Li, a substantial improvement in terms of cycling stability and lower overpotential with a stable cycling for more than 300 h is observed for the latter (Figure 5a). In contrast, the p-Li symmetric cell shows a dramatic increase in overpotential and eventually fades after only 12 cycles (ca. 80 h), suggesting that no electrochemically active lithium is left owing to the reaction with the liquid electrolyte. The tests with the 20 μm thick lithium foil (ca. 4 mAh cm^{-2}; Figure S8a) show essentially the same trend, with the p-Li cell fading after only 10 cycles. Figure S8b displays a magnification of the 1st and 10th stripping/

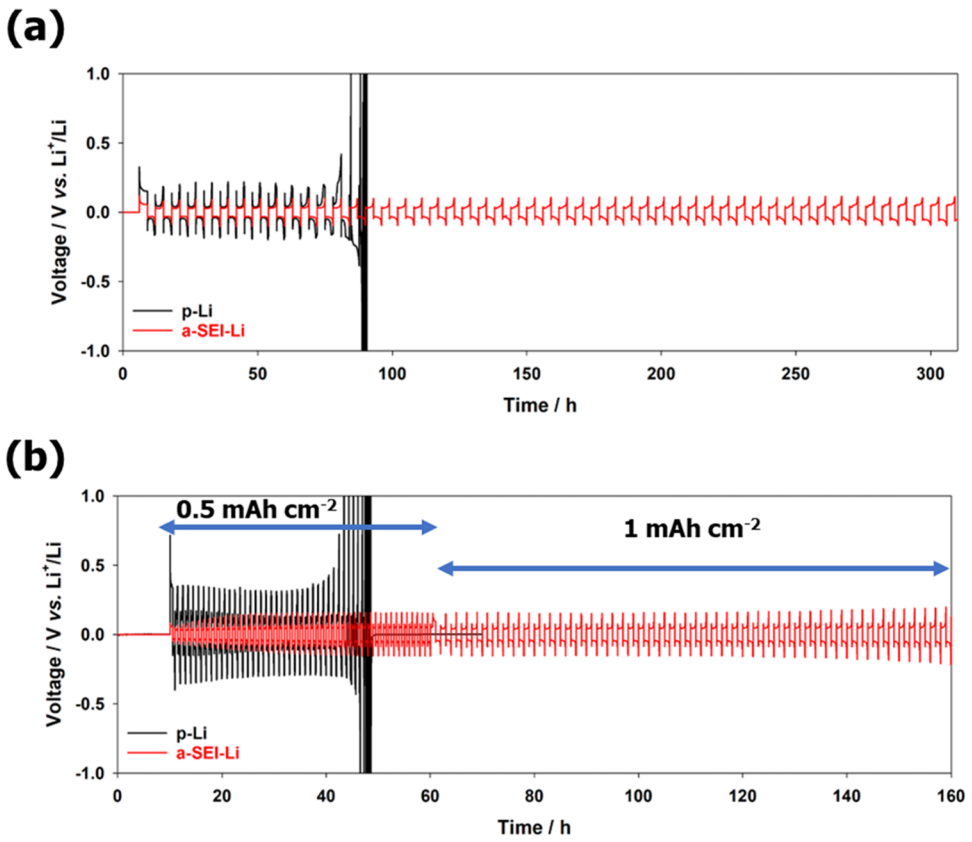

Figure 5. (a) Galvanostatic lithium stripping/plating experiments performed with p-Li (in black) and a-SEI-Li (in red) in symmetric Li||Li cells at a current density of 1.0 mA cm^{-2}, with each stripping and plating step lasting 3 h (3.0 mAh cm^{-2}). (b) Galvanostatic lithium stripping/plating tests conducted for p- (in black) and the a-SEI-coated 7 μm thick lithium foil in symmetric Li||Li cells at a current density of 1.0 mA cm^{-2}, with each plating and stripping step lasting 0.5 h (0.5 mAh cm^{-2}) for the first 50 cycles and 1 h (1.0 mAh cm^{-2}) for the subsequent cycles. Initial Li foil thickness: 50 μm; electrolyte: 60 μL; temperature: 20 ± 1 °C.

plating cycle, highlighting the higher overpotential and poorer reversibility, i.e., Coulombic efficiency, for p-Li. The results obtained for the 10 μm thick lithium foil (ca. 2 mAh cm^{-2}; Figure S8c) and for the 7 μm thick lithium foil (ca. 1.4 mAh cm^{-2}; Figure 5b) are further confirming the beneficial impact of a-SEI. The latter results are particularly remarkable, as a large fraction of the metallic lithium reacted with $SnCl_2$ and $LiNO_3$ (Figure 5), thus substantially reducing the amount of electrochemically active lithium available in the cell.

To further corroborate the beneficial impact of a-SEI on thinner Li electrodes, Li||NCM_{811} full-cells were assembled employing p-Li and a-SEI-Li made from 50 and 7 μm thick lithium foils. The results of the galvanostatic stripping/plating cycles are illustrated in Figure 6. It should be noted that the electrolyte volume/cathode areal capacity ratio was kept low, with about 20 μL per mAh in both cases. This is still rather high compared to commercial LIBs (though one also has to consider the different packing density inside the cell), but among the lowest values published in academic studies so far.[69] The capacity ratio (i.e., the N/P ratio) of the negative and positive electrode was rather low with about 3.2 and 0.44 for the Li||NCM_{811} cells comprising the 50 and 7 μm thick lithium foil, respectively—not considering the consumption of metallic lithium for the formation of a-SEI, which is of particular relevance for the 7 μm thick lithium foil. Independent from this, the N/P ratio of 0.44 in this case is one of the lowest that has been reported so far[66]—considering the consumption of metallic lithium for the formation of a-SEI presumably the lowest.

In the case of the 50 μm thick lithium foil, the Li||NCM_{811} cell containing p-Li faded after only 35 cycles, while the cell comprising a-SEI-Li foil provides a stable cycling for more than 80 cycles (Figure 6a). Selected dis-/charge profiles for the p-Li and a-SEI-Li cells are presented in Figure 6b,c. In the former case, the polarization rises dramatically along with the capacity fading (Figure 6b), presumably owing to the depletion of electrochemically active lithium and ongoing electrolyte decomposition, while it remains rather constant in the latter case (Figure 6c). Similarly, the application of a-SEI leads to a substantial improvement of the Li||NCM_{811} cell cycling stability based on the 7 μm thick lithium foil (Figure 6d), which is particularly remarkable considering the very limited amount of "excess" lithium in this cell. The a-SEI-Li cell shows a much lower fading after a stable cycling for more than 20 cycles, while the p-Li cell quickly fades within 10 cycles. The superior performance of a-SEI-Li is also reflected by substantially lower polarization (Figure 6e,f).

Given the aforementioned, very limited "excess" lithium in the a-SEI-Li made from 7 μm thick lithium foil and the extensive interest in so-called "anode-free" or "zero-excess" lithium batteries,[70] asymmetric Cu||Li were assembled and tested to compare p-Li and a-SEI-Li (Figure S9). The cell comprising a-SEI-Li shows a substantially enhanced reversibility and much lower polarization upon lithium stripping/plating test than that employing p-Li. This latter fades after

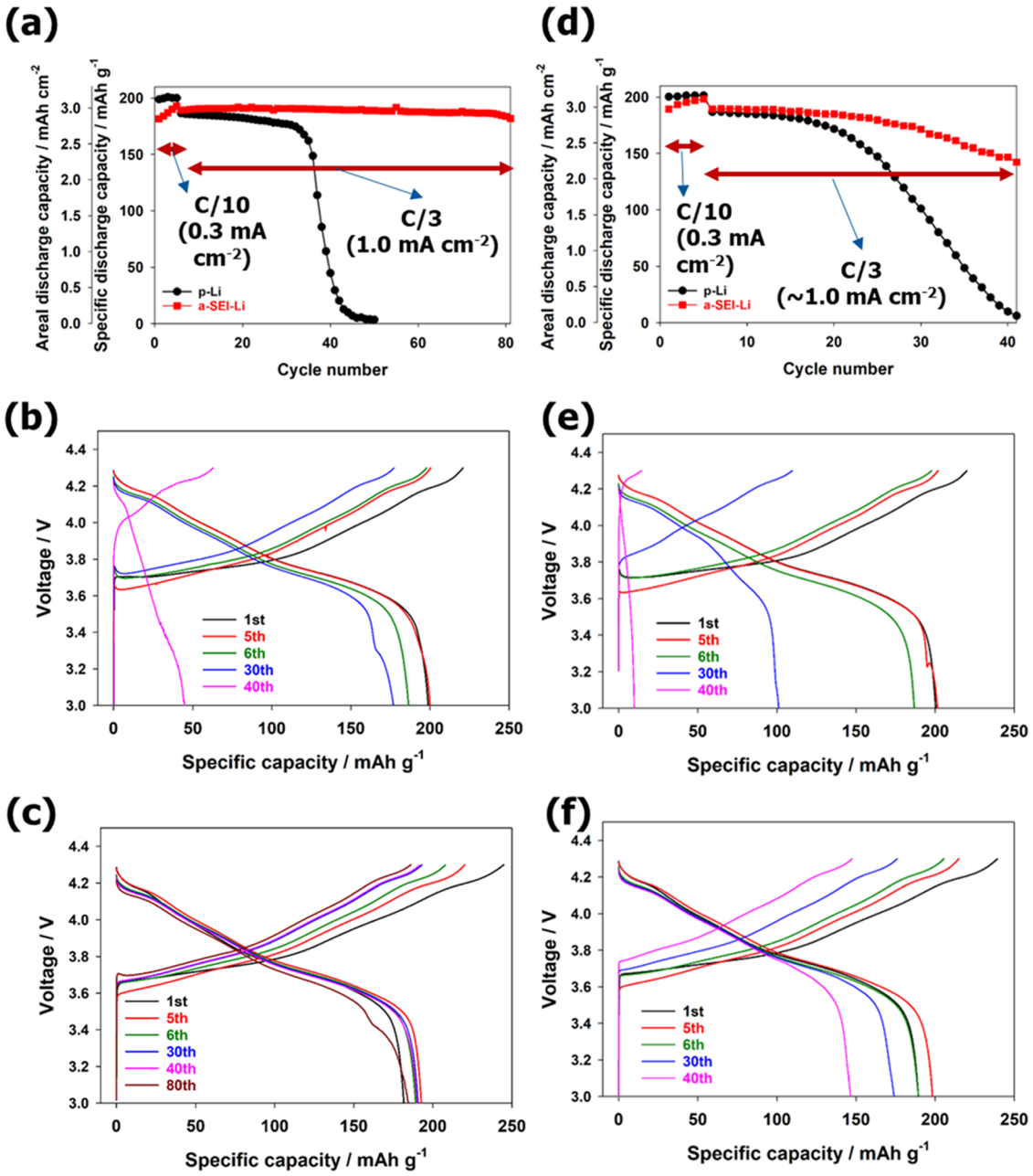

Figure 6. Galvanostatic cycling of (a-SEI-coated) Li||NCM_{811} cells based on (a–c) 50 μm and (d–f) 7 μm thick lithium foil, with (a, d) the plot of the areal and specific capacity as a function of cycle number as well as (b, c and e, f) selected dis-/charge profiles for the Li||NCM_{811} cells containing (b, e) p-Li and (c, f) the a-SEI-coated Li. The current density in the first five cycles was 0.3 mA cm^{-2} (C/10) and 1.0 mA cm^{-2} (C/3) in the following cycles. Electrolyte: 60 μL; temperature: 20 ± 1 °C.

only 15 cycles, while a-SEI-Li enables rather a stable cycling for more than 50 cycles, further underlining the advantageous effect of a-SEI for lithium-metal batteries.

CONCLUSIONS

A new artificial interphase (a-SEI) for lithium-metal electrodes has been presented. This a-SEI is based on a combination of inorganic and organic components derived from treating the lithium foil with a DME solution of $SnCl_2$ and $LiNO_3$. The results show that both inorganic precursors are essential for the realization of the advanced a-SEI, allowing for the long-term stable stripping and plating of metallic lithium—using several initial lithium foil thicknesses, varying from 300 to 50 and 20 and even as little as 10 and 7 μm. In the latter case, the great majority of metallic lithium is consumed for the formation of a-SEI, rendering the substantial improvement in lithium stripping/plating reversibility in symmetric cells even more remarkable. This advantageous effect is further corroborated by the great improvement in cycling stability and reversibility of Li||NCM_{811} full-cells and asymmetric Cu||Li cells. Noteworthy, the N/P ratio of the Li||NCM_{811} full-cells comprising the 7 μm thick lithium foil is as low as 0.44—and even much lower in the case of a-SEI-Li, making these cells very close to the so-called “anode-free” or “zero-excess” lithium batteries and further underlining the highly beneficial impact of this a-SEI.

AUTHOR INFORMATION

Corresponding Authors

Dominic Bresser − *Helmholtz Institute Ulm (HIU), 89081 Ulm, Germany; Karlsruhe Institute of Technology (KIT), 76021 Karlsruhe, Germany;* orcid.org/0000-0001-6429-6048; Email: dominic.bresser@kit.edu

Stefano Passerini − *Helmholtz Institute Ulm (HIU), 89081 Ulm, Germany; Karlsruhe Institute of Technology (KIT), 76021 Karlsruhe, Germany; Chemistry Department, Sapienza University of Rome, 00185 Rome, Italy;* orcid.org/0000-0002-6606-5304; Email: stefano.passerini@kit.edu

Authors

Yongil Kim − *Helmholtz Institute Ulm (HIU), 89081 Ulm, Germany; Karlsruhe Institute of Technology (KIT), 76021 Karlsruhe, Germany; Research Institute of Industrial Science and Technology (RIST), 21985 Incheon, Republic of Korea*

Dominik Stepien − *Helmholtz Institute Ulm (HIU), 89081 Ulm, Germany; Karlsruhe Institute of Technology (KIT), 76021 Karlsruhe, Germany*

Hyein Moon − *Helmholtz Institute Ulm (HIU), 89081 Ulm, Germany; Karlsruhe Institute of Technology (KIT), 76021 Karlsruhe, Germany*

Kay Schönherr − *Fraunhofer Institute for Material and Beam Technology (IWS), 01277 Dresden, Germany;* orcid.org/0000-0002-7880-9120

Benjamin Schumm − *Fraunhofer Institute for Material and Beam Technology (IWS), 01277 Dresden, Germany*

Matthias Kuenzel − *Helmholtz Institute Ulm (HIU), 89081 Ulm, Germany; Karlsruhe Institute of Technology (KIT), 76021 Karlsruhe, Germany*

Holger Althues − *Fraunhofer Institute for Material and Beam Technology (IWS), 01277 Dresden, Germany;* orcid.org/0000-0002-3865-6262

Notes

The authors declare no competing financial interest.

ACKNOWLEDGMENTS

Y.K., D.S., H.M., M.K., D.B., and S.P. would like to acknowledge financial support from the Helmholtz Association and the German Federal Ministry of Education and Research (BMBF) within the ExcellBattUlm project (03XP0257D). K.S. and H.A. would like to acknowledge financial support from the BMBF within the KaSiLi project (03XP0254A) and the MaLiBa project (03XP0185A). Moreover, the authors are very grateful to Dr. Zhen Chen for the preparation of the NCM_{811}-based electrodes and to Dr. Guk-Tae Kim and Prof. Jae-Kwang Kim for providing the NCM_{811} active material.

REFERENCES

(1) Tarascon, J. M.; Armand, M. Issues and Challenges Facing Rechargeable Lithium Batteries. *Nature* **2001**, *414*, 359−367.

(2) Dunn, B.; Kamath, H.; Tarascon, J.-M. Electrical Energy Storage for the Grid: A Battery of Choices. *Science* **2011**, *334*, 928−935.

(3) Marinaro, M.; Bresser, D.; Beyer, E.; Faguy, P.; Hosoi, K.; Li, H.; Sakovica, J.; Amine, K.; Wohlfahrt-Mehrens, M.; Passerini, S. Bringing Forward the Development of Battery Cells for Automotive Applications: Perspective of R&D Activities in China, Japan, the EU and the USA. *J. Power Sources* **2020**, *459*, No. 228073.

(4) Choi, J. W.; Aurbach, D. Promise and Reality of Post-lithium-ion Batteries with High Energy Densities. *Nat. Rev. Mater.* **2016**, *1*, No. 16013.

(5) Goodenough, J. B.; Kim, Y. Challenges for Rechargeable Li Batteries. *Chem. Mater.* **2010**, *22*, 587−603.

(6) Goodenough, J. B. Electrochemical Energy Storage in a Sustainable Modern Society. *Energy Environ. Sci.* **2014**, *7*, 14−18.

(7) Gao, J.; Shi, S.-Q.; Li, H. Brief Overview of Electrochemical Potential in Lithium Ion Batteries. *Chin. Phys. B* **2016**, *25*, No. 018210.

(8) Liu, J.; Bao, Z.; Cui, Y.; Dufek, E. J.; Goodenough, J. B.; Khalifah, P.; Li, Q.; Liaw, B. Y.; Liu, P.; Manthiram, A.; Meng, Y. S.; Subramanian, V. R.; Toney, M. F.; Viswanathan, V. V.; Whittingham, M. S.; Xiao, J.; Xu, W.; Yang, J.; Yang, X.-Q.; Zhang, J.-G. Pathways for Practical High-energy Long-cycling Lithium Metal Batteries. *Nat. Energy* **2019**, *4*, 180−186.

(9) He, X.; Bresser, D.; Passerini, S.; Baakes, F.; Krewer, U.; Lopez, J.; Mallia, C. T.; Shao-Horn, Y.; Cekic-Laskovic, I.; Wiemers-Meyer, S.; Soto, F. A.; Ponce, V.; Seminario, J. M.; Balbuena, P. B.; Jia, H.; Xu, W.; Xu, Y.; Wang, C.; Horstmann, B.; Amine, R.; Su, C.-C.; Shi, J.; Amine, K.; Winter, M.; Latz, A.; Kostecki, R. The Passivity of Lithium Electrodes in Liquid Electrolytes for Secondary Batteries. *Nat. Rev. Mater.* **2021**, *6*, 1036−1052.

(10) Xu, W.; Wang, J.; Ding, F.; Chen, X.; Nasybulin, E.; Zhang, Y.; Zhang, J.-G. Lithium Metal Anodes for Rechargeable Batteries. *Energy Environ. Sci.* **2014**, *7*, 513−537.

(11) Lin, D.; Liu, Y.; Cui, Y. Reviving the Lithium Metal Anode for High-energy Batteries. *Nat. Nanotechnol.* **2017**, *12*, 194−206.

(12) Shen, X.; Liu, H.; Cheng, X.-B.; Yan, C.; Huang, J.-Q. Beyond Lithium Ion Batteries: Higher Energy Density Battery Systems Based on Lithium Metal Anodes. *Energy Storage Mater.* **2018**, *12*, 161−175.

(13) Wang, Z.; Wang, Y.; Wu, C.; Pang, W. K.; Mao, J.; Guo, Z. Constructing Nitrided Interfaces for Stabilizing Li Metal Electrodes in Liquid Electrolytes. *Chem. Sci.* **2021**, *12*, 8945−8966.

(14) Whittingham, M. S. Electrical Energy Storage and Intercalation Chemistry. *Science* **1976**, *192*, 1126−1127.

(15) Yoshino, A. The Birth of the Lithium-Ion Battery. *Angew. Chem., Int. Ed.* **2012**, *51*, 5798−5800.

(16) Horstmann, B.; Shi, J.; Amine, R.; Werres, M.; He, X.; Jia, H.; Hausen, F.; Cekic-Laskovic, I.; Wiemers-Meyer, S.; Lopez, J.; Galvez-Aranda, D.; Baakes, F.; Bresser, D.; Su, C.-C.; Xu, Y.; Xu, W.; Jakes, P.; Eichel, R.-A.; Figgemeier, E.; Krewer, U.; Seminario, J. M.; Balbuena, P. B.; Wang, C.; Passerini, S.; Shao-Horn, Y.; Winter, M.; Amine, K.; Kostecki, R.; Latz, A. Strategies Towards Enabling Lithium Metal in Batteries: Interphases and Electrodes. *Energy Environ. Sci.* **2021**, *14*, 5289−5314.

(17) Varzi, A.; Thanner, K.; Scipioni, R.; Di Lecce, D.; Hassoun, J.; Dörfler, S.; Altheus, H.; Kaskel, S.; Prehal, C.; Freunberger, S. A. Current Status and Future Perspectives of Lithium Metal Batteries. *J. Power Sources* **2020**, *480*, No. 228803.

(18) Cheng, X.-B.; Zhang, R.; Zhao, C.-Z.; Zhang, Q. Toward Safe Lithium Metal Anode in Rechargeable Batteries: A Review. *Chem. Rev.* **2017**, *117*, 10403−10473.

(19) Peled, E. The Electrochemical Behavior of Alkali and Alkaline Earth Metals in Nonaqueous Battery Systems—The Solid Electrolyte Interphase Model. *J. Electrochem. Soc.* **1979**, *126*, 2047−2051.

(20) Peled, E. Film Forming Reaction at the Lithium/electrolyte Interface. *J. Power Sources* **1983**, *9*, 253−266.

(21) Aurbach, D. Review of Selected Electrode−solution Interactions Which Determine the Performance of Li and Li Ion Batteries. *J. Power Sources* **2000**, *89*, 206−218.
(22) Zhang, H.; Eshetu, G. G.; Judez, X.; Li, C.; Rodriguez-Martínez, L. M.; Armand, M. Electrolyte Additives for Lithium Metal Anodes and Rechargeable Lithium Metal Batteries: Progress and Perspectives. *Angew. Chem., Int. Ed.* **2018**, *57*, 15002−15027.
(23) Zhai, P.; Liu, L.; Gu, X.; Wang, T.; Gong, Y. Interface Engineering for Lithium Metal Anodes in Liquid Electrolyte. *Adv. Energy Mater.* **2020**, *10*, No. 2001257.
(24) Li, S.; Jiang, M.; Xie, Y.; Xu, H.; Jia, J.; Li, J. Developing High-Performance Lithium Metal Anode in Liquid Electrolytes: Challenges and Progress. *Adv. Mater.* **2018**, *30*, No. 1706375.
(25) Jin, D.; Park, J.; Ryou, M.-H.; Lee, Y. M. Structure-Controlled Li Metal Electrodes for Post-Li-Ion Batteries: Recent Progress and Perspectives. *Adv. Mater. Interfaces* **2020**, *7*, No. 1902113.
(26) Popovic, J. The Importance of Electrode Interfaces and Interphases for Rechargeable Metal Batteries. *Nat. Commun.* **2021**, *12*, No. 6240.
(27) Yu, Z.; Cui, Y.; Bao, Z. Design Principles of Artificial Solid Electrolyte Interphases for Lithium-Metal Anodes. *Cell Rep. Phys. Sci.* **2020**, *1*, No. 100119.
(28) Kang, D.; Xiao, M.; Lemmon, J. P. Artificial Solid-Electrolyte Interphase for Lithium Metal Batteries. *Batteries Supercaps* **2021**, *4*, 445−455.
(29) Gao, S.; Sun, F.; Liu, N.; Yang, H.; Cao, P.-F. Ionic Conductive Polymers as Artificial Solid Electrolyte Interphase Films in Li Metal Batteries − A review. *Mater. Today* **2020**, *40*, 140−159.
(30) Cheng, X.-B.; Yan, C.; Chen, X.; Guan, C.; Huang, J.-Q.; Peng, H.-J.; Zhang, R.; Yang, S.-T.; Zhang, Q. Implantable Solid Electrolyte Interphase in Lithium-Metal Batteries. *Chem* **2017**, *2*, 258−270.
(31) Xu, R.; Cheng, X.-B.; Yan, C.; Zhang, X.-Q.; Xiao, Y.; Zhao, C.-Z.; Huang, J.-Q.; Zhang, Q. Artificial Interphases for Highly Stable Lithium Metal Anode. *Matter* **2019**, *1*, 317−344.
(32) Touja, J.; Louvain, N.; Stievano, L.; Monconduit, L.; Berthelot, R. An Overview on Protecting Metal Anodes with Alloy-Type Coating. *Batteries Supercaps* **2021**, *4*, 1252−1266.
(33) Liu, H.; Cheng, X.-B.; Huang, J.-Q.; Kaskel, S.; Chou, S.; Park, H. S.; Zhang, Q. Alloy Anodes for Rechargeable Alkali-Metal Batteries: Progress and Challenge. *ACS Mater. Lett.* **2019**, *1*, 217−229.
(34) Liang, X.; Pang, Q.; Kochetkov, I. R.; Sempere, M. S.; Huang, H.; Sun, X.; Nazar, L. F. A Facile Surface Chemistry Route to a Stabilized Lithium Metal Anode. *Nat. Energy* **2017**, *2*, No. 17119.
(35) Tu, Z.; Choudhury, S.; Zachman, M. J.; Wei, S.; Zhang, K.; Kourkoutis, L. F.; Archer, L. A. Fast Ion Transport at Solid−solid Interfaces in Hybrid Battery Anodes. *Nat. Energy* **2018**, *3*, 310−316.
(36) Lee, Y.-G.; Fujiki, S.; Jung, C.; Suzuki, N.; Yashiro, N.; Omoda, R.; Ko, D.-S.; Shiratsuchi, T.; Sugimoto, T.; Ryu, S.; Ku, J. H.; Watanabe, T.; Park, Y.; Aihara, Y.; Im, D.; Han, I. T. High-energy Long-cycling All-solid-state Lithium Metal Batteries Enabled by Silver−carbon Composite Anodes. *Nat. Energy* **2020**, *5*, 299−308.
(37) Pang, Q.; Liang, X.; Kochetkov, I. R.; Hartmann, P.; Nazar, L. F. Stabilizing Lithium Plating by a Biphasic Surface Layer Formed In Situ. *Angew. Chem., Int. Ed.* **2018**, *57*, 9795−9798.
(38) Zhao, Q.; Tu, Z.; Wei, S.; Zhang, K.; Choudhury, S.; Liu, X.; Archer, L. A. Building Organic/Inorganic Hybrid Interphases for Fast Interfacial Transport in Rechargeable Metal Batteries. *Angew. Chem., Int. Ed.* **2018**, *57*, 992−996.
(39) Thanner, K.; Varzi, A.; Buchholz, D.; Sedlmaier, S. J.; Passerini, S. Artificial Solid Electrolyte Interphases for Lithium Metal Electrodes by Wet Processing: The Role of Metal Salt Concentration and Solvent Choice. *ACS Appl. Mater. Interfaces* **2020**, *12*, 32851−32862.
(40) Kim, Y.; Koo, D.; Ha, S.; Jung, S. C.; Yim, T.; Kim, H.; Oh, S. K.; Kim, D.-M.; Choi, A.; Kang, Y.; Ryu, K. H.; Jang, M.; Han, Y.-K.; Oh, S. M.; Lee, K. T. Two-Dimensional Phosphorene-Derived Protective Layers on a Lithium Metal Anode for Lithium-Oxygen Batteries. *ACS Nano* **2018**, *12*, 4419−4430.
(41) Kwon, B.; Ha, S.; Kim, D.-M.; Koo, D.; Lee, J.; Lee, K. T. Electrochemically Active Red P/BaTiO3-Based Protective Layers Suppressing Li Dendrite Growth for Li Metal Batteries. *Adv. Mater. Interfaces* **2020**, *7*, No. 2001037.
(42) Xu, B.; Liu, Z.; Li, J.; Huang, X.; Qie, B.; Gong, T.; Tan, L.; Yang, X.; Paley, D.; Dontigny, M.; Zaghib, K.; Liao, X.; Cheng, Q.; Zhai, H.; Chen, X.; Chen, L.-Q.; Nan, C.-W.; Lin, Y.-H.; Yang, Y. Engineering Interfacial Adhesion for High-performance Lithium Metal Anode. *Nano Energy* **2020**, *67*, No. 104242.
(43) Chen, T.; Kong, W.; Zhao, P.; Lin, H.; Hu, Y.; Chen, R.; Yan, W.; Jin, Z. Dendrite-Free and Stable Lithium Metal Anodes Enabled by an Antimony-Based Lithiophilic Interphase. *Chem. Mater.* **2019**, *31*, 7565−7573.
(44) Aurbach, D.; Pollak, E.; Elazari, R.; Salitra, G.; Kelley, C. S.; Affinito, J. On the Surface Chemical Aspects of Very High Energy Density, Rechargeable Li−Sulfur Batteries. *J. Electrochem. Soc.* **2009**, *156*, No. A694.
(45) Zhang, S. S. Role of LiNO3 in Rechargeable Lithium/sulfur Battery. *Electrochim. Acta* **2012**, *70*, 344−348.
(46) Xiong, S.; Xie, K.; Diao, Y.; Hong, X. Properties of Surface Film on Lithium Anode with LiNO3 as Lithium Salt in Electrolyte Solution for Lithium−sulfur Batteries. *Electrochim. Acta* **2012**, *83*, 78−86.
(47) Li, W.; Yao, H.; Yan, K.; Zheng, G.; Liang, Z.; Chiang, Y.-M.; Cui, Y. The Synergetic Effect of Lithium Polysulfide and Lithium Nitrate to Prevent Lithium Dendrite Growth. *Nat. Commun.* **2015**, *6*, No. 7436.
(48) Erickson, E. M.; Markevich, E.; Salitra, G.; Sharon, D.; Hirshberg, D.; de la Llave, E.; Shterenberg, I.; Rosenman, A.; Frimer, A.; Aurbach, D. Review—Development of Advanced Rechargeable Batteries: A Continuous Challenge in the Choice of Suitable Electrolyte Solutions. *J. Electrochem. Soc.* **2015**, *162*, A2424−A2438.
(49) Shi, Q.; Zhong, Y.; Wu, M.; Wang, H.; Wang, H. High-capacity Rechargeable Batteries Based on Deeply Cyclable Lithium Metal Anodes. *Proc. Natl. Acad. Sci. U.S.A.* **2018**, *115*, 5676−5680.
(50) Zhang, X.-Q.; Chen, X.; Cheng, X.-B.; Li, B.-Q.; Shen, X.; Yan, C.; Huang, J.-Q.; Zhang, Q. Highly Stable Lithium Metal Batteries Enabled by Regulating the Solvation of Lithium Ions in Nonaqueous Electrolytes. *Angew. Chem., Int. Ed.* **2018**, *57*, 5301−5305.
(51) Miao, R.; Yang, J.; Feng, X.; Jia, H.; Wang, J.; Nuli, Y. Novel Dual-salts Electrolyte Solution for Dendrite-free Lithium-metal Based Rechargeable Batteries with High Cycle Reversibility. *J. Power Sources* **2014**, *271*, 291−297.
(52) Schönherr, K.; Schumm, B.; Hippauf, F.; Lissy, R.; Althues, H.; Leyens, C.; Kaskel, S. Liquid Lithium Metal Processing into Ultrathin Metal Anodes for Solid State Batteries. *Chem. Eng. J. Adv.* **2022**, *9*, No. 100218.
(53) Yin, Y.-C.; Wang, Q.; Yang, J.-T.; Li, F.; Zhang, G.; Jiang, C.-H.; Mo, H.-S.; Yao, J.-S.; Wang, K.-H.; Zhou, F.; Ju, H.-X.; Yao, H.-B. Metal Chloride Perovskite Thin Film Based Interfacial Layer for Shielding Lithium Metal from Liquid Electrolyte. *Nat. Commun.* **2020**, *11*, No. 1761.
(54) Lin, L.; Liang, F.; Zhang, K.; Mao, H.; Yang, J.; Qian, Y. Lithium Phosphide/lithium Chloride Coating on Lithium for Advanced Lithium Metal Anode. *J. Mater. Chem. A* **2018**, *6*, 15859−15867.
(55) Zheng, X.; Fu, H.; Hu, C.; Xu, H.; Huang, Y.; Wen, J.; Sun, H.; Luo, W.; Huang, Y. Toward a Stable Sodium Metal Anode in Carbonate Electrolyte: A Compact, Inorganic Alloy Interface. *J. Phy. Chem. Lett.* **2019**, *10*, 707−714.
(56) Chen, Q.; He, H.; Hou, Z.; Zhuang, W.; Zhang, T.; Sun, Z.; Huang, L. Building an Artificial Solid Electrolyte Interphase With High-uniformity and Fast Ion Diffusion for Ultralong-life Sodium Metal Anodes. *J. Mater. Chem. A* **2020**, *8*, 16232−16237.
(57) Jin, D.; Roh, Y.; Jo, T.; Ryou, M.-H.; Lee, H.; Lee, Y. M. Robust Cycling of Ultrathin Li Metal Enabled by Nitrate-Preplanted Li Powder Composite. *Adv. Energy Mater.* **2021**, *11*, No. 2003769.
(58) Krauskopf, T.; Richter, F. H.; Zeier, W. G.; Janek, J. Physicochemical Concepts of the Lithium Metal Anode in Solid-State Batteries. *Chem. Rev.* **2020**, *120*, 7745−7794.

(59) Zhu, Y.; He, X.; Mo, Y. Origin of Outstanding Stability in the Lithium Solid Electrolyte Materials: Insights from Thermodynamic Analyses Based on First-Principles Calculations. *ACS Appl. Mater. Interfaces* **2015**, *7*, 23685−23693.
(60) Wood, K. N.; Noked, M.; Dasgupta, N. P. Lithium Metal Anodes: Toward an Improved Understanding of Coupled Morphological, Electrochemical, and Mechanical Behavior. *ACS Energy Lett.* **2017**, *2*, 664−672.
(61) Ota, H.; Shima, K.; Ue, M.; Yamaki, J.-i. Effect of Vinylene Carbonate as Additive to Electrolyte for Lithium Metal Anode. *Electrochim. Acta* **2004**, *49*, 565−572.
(62) Ota, H.; Sakata, Y.; Otake, Y.; Shima, K.; Ue, M.; Yamaki, J.-i. Structural and Functional Analysis of Surface Film on Li Anode in Vinylene Carbonate-Containing Electrolyte. *J. Electrochem. Soc.* **2004**, *151*, No. A1778.
(63) Kitz, P. G.; Lacey, M. J.; Novák, P.; Berg, E. J. Operando Investigation of the Solid Electrolyte Interphase Mechanical and Transport Properties Formed from Vinylene Carbonate and Fluoroethylene Carbonate. *J. Power Sources* **2020**, *477*, No. 228567.
(64) Ding, M. S.; Koch, S. L.; Passerini, S. The Effect of 1-Pentylamine as Solid Electrolyte Interphase Precursor on Lithium Metal Anodes. *Electrochim. Acta* **2017**, *240*, 408−414.
(65) Wang, L.; Zhang, L.; Wang, Q.; Li, W.; Wu, B.; Jia, W.; Wang, Y.; Li, J.; Li, H. Long Lifespan Lithium Metal Anodes Enabled by Al2O3 Sputter Coating. *Energy Storage Mater.* **2018**, *10*, 16−23.
(66) Ue, M.; Sakaushi, K.; Uosaki, K. Basic Knowledge in Battery Research Bridging the Gap Between Academia and Industry. *Mater. Horiz.* **2020**, *7*, 1937−1954.
(67) Niu, C.; Lee, H.; Chen, S.; Li, Q.; Du, J.; Xu, W.; Zhang, J.-G.; Whittingham, M. S.; Xiao, J.; Liu, J. High-energy Lithium Metal Pouch Cells with Limited Anode Swelling and Long Stable Cycles. *Nat. Energy* **2019**, *4*, 551−559.
(68) Ren, X.; Zou, L.; Cao, X.; Engelhard, M. H.; Liu, W.; Burton, S. D.; Lee, H.; Niu, C.; Matthews, B. E.; Zhu, Z.; Wang, C.; Arey, B. W.; Xiao, J.; Liu, J.; Zhang, J.-G.; Xu, W. Enabling High-Voltage Lithium-Metal Batteries under Practical Conditions. *Joule* **2019**, *3*, 1662−1676.
(69) Lee, S. H.; Hwang, J.-Y.; Ming, J.; Kim, H.; Jung, H.-G.; Sun, Y.-K. Long-Lasting Solid Electrolyte Interphase for Stable Li-Metal Batteries. *ACS Energy Lett.* **2021**, *6*, 2153−2161.
(70) Nanda, S.; Gupta, A.; Manthiram, A. Anode-Free Full Cells: A Pathway to High-Energy Density Lithium-Metal Batteries. *Adv. Energy Mater.* **2021**, *11*, No. 2000804.